90th Anniversary of the Department of Physical Chemistry of the University of Sofia
Юбилей: 90 години на Катедрата по физикохимия на Софийския университет

INTERFACIAL REORGANIZATION OF MOLECULAR ASSEMBLIES USED AS DRUG DELIVERY SYSTEMS

I. Panaiotov, Tz. Ivanova, K. Balashev, N. Grozev, I. Minkov, K. Mircheva
University of Sofia, Bulgaria

Abstract. The number of potential applications of nanosized molecular assemblies such as vesicles, nanocapsules, biodegradable polyester matrix and more complex structures in drug research and nanomedicine is rapidly increasing with the developed technologies to tune and control their bulk and mainly surface properties. For a better understanding of nanoparticle behavior at the membrane interfaces an *in vitro* study of the mechanisms of loss of mechanical stability and their reorganization on various membrane systems seems indispensable. By using the simplest convenient monolayer models the mechanisms of destabilization and reorganization of various classical or modified nanosized molecular assemblies spread or adsorbed on pure air/water interface or at the preformed model membrane were studied.

Keywords: vesicles, lipid nanocapsules, lung surfactants, spreading, model membrane monolayer

Introduction

Nowadays a real revolution in galenics occurs. The traditional forms of drug administration give up one's place to the new drug delivery systems (DDS). During the last decades, an important progress has been made by tailoring various kinds

of micro- and nanosized molecular assemblies (MA) used as drug carriers (Fig.1): the well known small unilamellar vesicles (SUV) used for many pharmaceutical purposes (Szoka, 1991; Sharma & Sharma, 1997) ; the lipid nanocapsules (LNC) with a core of triglycerides (TG) covered by a soft layer of polyethylene glycol (PEG) and stabilized by phospholipids (PL) (Heurtault et al., 2002; Malzert-Freon et al., 2010); the biodegradable polyester matrix of poly (α-hydroxy acid)s - PLA, PLAGA or PLA-PEG copolymer also among the most widely used DDS namely for local treatment of cancer (Makadia & Siegel, 2011; Kumari et al., 2010; Glowka et al., 2010); more complex structures of commercially available lung surfactant (LS), containing phospholipids (PL) and proteins (P) clinically administrated to treat the neonatal respiratory distress syndrome (NRDS) (Notter, 2000; Lalchev & Christova; 2010; Blanco & Perez-Gil, 2007); the coacervates containing plant proteins like α-gliadin (Ducel et al., 2004) and cage molecules like β-cyclodextrin (β-CD) used to protect sensitive substances such as vitamins etc. (Yuan et al., 2008; Zaibunnisa et al., 2011; Arun Rasheed et al., 2008). From the physicochemical point of view, a better understanding of mechanisms of formulation of such nanosized structures and their behavior in living environment seems indispensable. Despite the complexity of the living systems, it is possible to produce generic models of MA reorganization at membrane interfaces by considering simple model systems. The present article generalizes some ideas and examples about the loss of mechanical stability and reorganization of SUV, LNC, PLA matrix, LS at model membrane interfaces obtained in a series of investigations in Laboratory of Biophysical Chemistry in close collaboration with J.E. Proust, P. Saulnier, F. Boury, F. Lagarce and A.C. Groo from the French Laboratory of University of Angers. More attention will be paid to recently studied case of interaction between the Paclitaxel (Ptx)-loaded LNC and 2D and 3D-mucus membrane models. The theoretical description takes into account the coupling of various processes when MA were spread or adsorbed at A/W or O/W interfaces or at 2D- and 3D- model membrane interfaces.

Materials and methods

Materials

Dioleoylphosphatidylcholine (DOPC), dipalmitoylphosphatidylcholine (DPPC), bovine serum albumin (BSA), polyvinylpyrrolidone (PVP), polyethylene glycol (PEG), porcine pancreatic phospholipase A_2 and Sepharose® CL4-B column from Sigma - Aldrich were used.

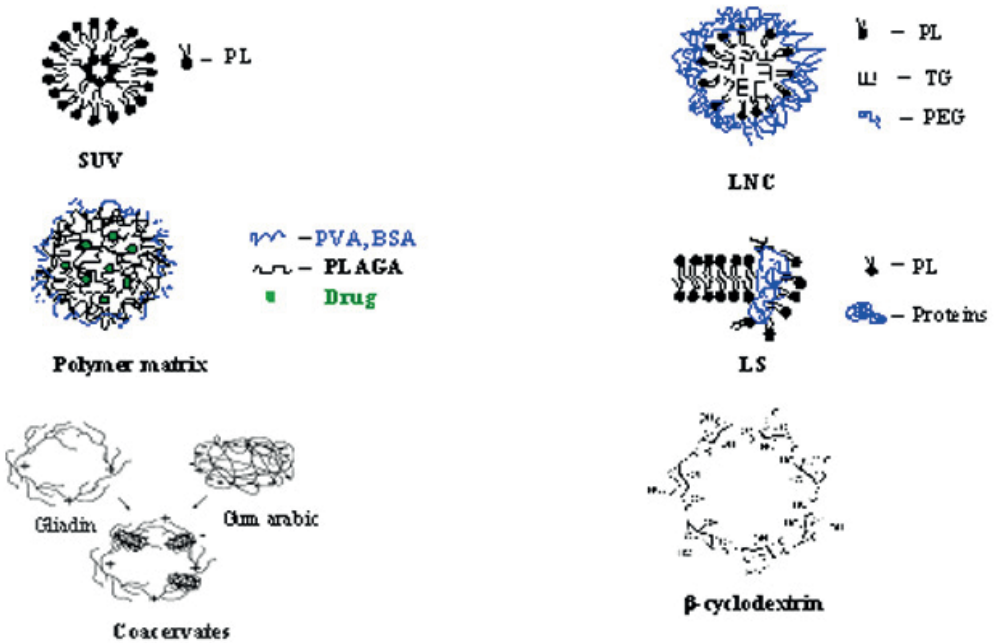

Fig. 1. Scheme of different nanosized assemblies

Poly (D,L-lactic acid) (PLA 50) stereocopolymer was obtained from CRBPA (Montpellier, France).

Dichloromethane (DCM) was supplied by Prolabo (Paris, France) and used without further purification.

Labrafac® WL1349-mixture from caprylic and capric acid triglycerides is provided by Gattefossé S.A. (Saint-Priest, France). Lipoid® S75-3- it contents soybean lecithin with 69% of phosphatidylcholine. It is a gift from Lipoid GmbH (Ludwigshafen, Germany). Solutol® HS15-mixture of free polyethylene glycol 660 (30%) and 12-hydroxystearate of polyethylene glycol 660 (70%) is provided by BASF (Ludwigshafen, Germany). NaCl is a product of Theokom (Sofia, Bulgaria). These products were used for LNC formulation.

Chloroform supplied from Merck (Germany) and Dichloromethane (DCM) from Prolabo (Paris, France) was used as spreading solvent.

Amphiphilic phospholipids with PEG used in the post-insertion are supplied by Avanti® Polar Lipids Ins. (USA): 1,2 Distearoyl-sn-glycero-3-phosphoethanolamine-N-

[methoxy(polyethylene-glycol)] with a PEG length 2000, 3000 and 5000 (DSPE-PEG-OCH_3), 1,2 Distearoyl-sn-glycero-3-phosphoethanolamine-N-[amino(polyethylene-glycol)] with a PEG length 2000, (DSPE-PEG-NH_2); DSPE-PEG-COOH.

Paclitaxel (Ptx) powder used for LNC formulation was obtained from Teva pharm (Opava-Komarov, Czech Republic). Injectable solution of Ptx at 6 mg/mL (Taxol®) was obtained from Bristol-Myers Squibb (Rueil-Malmaison, France). Purified water was obtained from a MilliQ185 System (Millipore, Paris, France). PBS buffer was obtained from Lonza (Verviers, Belgium).

Exosurf® Neonatal (Burroughs Welcome, Research Triangle Park, NC, USA): Purely synthetical, protein-free surfactant preparation. It contains about 80% dipalmitoylphosphatidylcholine (DPPC), combined with hexadecanol and tyloxapol added to partially overcome the bad spreading of DPPC.

Survanta® Beractant (Ross Laboratories, Columbus, Ohio): Semisynthetical surfactant, one of the most commonly used in the USA. It is a natural extract of bovine lung surfactant, containing 88% phospholipids (about 50% DPPC) and the hydrophobic lung surfactant proteins (about 1%).

Curosurf® (Chiesi Farmaceutici, Parma, Italy): Natural surfactant extract, prepared from porcine lungs, containing almost exclusively polar lipids in particular phosphatidylcholine (about 70% of total phospholipid content), phosphatidylglycerol (about 30% of total phospholipid content) and about 1% of hydrophobic proteins SP-B and SP-C.

Alveofact® (Lyomark Pharma): Natural surfactant extract, prepared from bovine lung containing 50–60 mg phospholipid faction, 5.4 mg NaCl and small amount of hydrophobic proteins SP-B and SP-C (about 1%).

Methods

To study the behavior of various molecular assemblies (MA) at air/water (A/W) or oil/water (O/W) interfaces two modes of deposition-spreading or adsorption from the MA aqueous suspension were used (Fig.2).

In the first a small quantity of the aqueous suspension with a given concentration was spread at A/W interface forming a layer with thickness *L*. In the second mode, the whole suspension was poured into the trough. In both cases the particles from the first subsurface layer undergo reorganization at the A/W pure interface leading to the formation of an interfacial layer (IL) with specific organization or interact with a prealably deposed model membrane monolayer. The PLA monolayer was spread at A/W interface from dichloromethane (DCM) solution.

The complex phenomena occurring during the MA reorganization at interfaces were followed by measuring the thermodynamical (surface tension -σ, surface pressure-π)

electrical (surface potential-ΔV) properties and kinetics of interfacial layer formation (the surface area change - ΔA with time t at constant π (Fig. 3A) (Verger & de Haas, 1973). The surface pressure (π) was measured using a KSV-2200 (Finland) surface balance, equipped with a platinum plate and a Teflon trough. The surface potential (ΔV) was measured simultaneously by using a gold-coated ^{241}Am ionizing electrode, a reference electrode and a KP 511 (Kriona, Bulgaria) electrometer, connected to a PC, provided with user software for real-time data measurements.

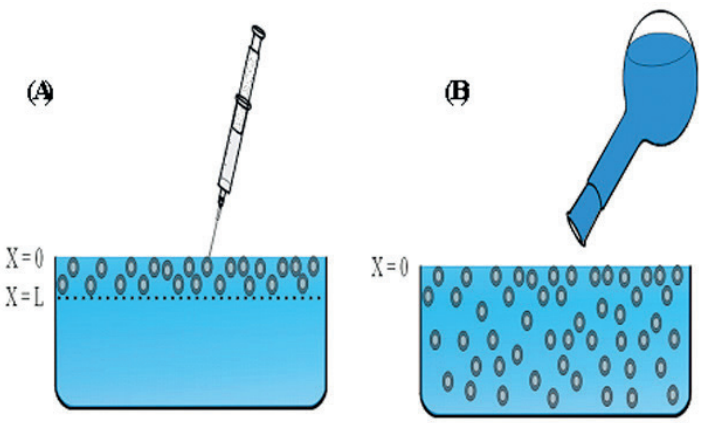

Fig. 2. Two procedures of formation of a surface film from SUV, LNC and LS aqueous dispersions. (**A**) - Spreading of a volume of dispersion at the air/water interface; (**B**) - Surface film is formed from the aqueous dispersion filled in a Teflon trough

The dilatational rheological properties of a monolayer (surface elasticity- E_d, characteristic times of the relaxation processes- θ and τ) were also studied (Figs. 3 B,C). The method consists of realizing small compressions (or expansions) of the monolayer by means of a barrier moving with a constant velocity U_b (Fig. 3Ba). As a result of the surface density gradient, caused by the continuous local surface pressure perturbation, a simultaneous motion of the monolayer and liquid substrate occurs (so-called Marangoni effect). The surface motion is practically dilatational and can be detected by measuring the change of any surface parameters. As shown in Fig.3Ba, the change in the local surface pressure is measured by using a Wilhelmy plate at points x_1, x_2 and x_3. A complete description of the simultaneous motion of the monolayer and liquid substrate was made (Panaiotov et al., 1979; Dimitrov et al., 1978); and summarized by Panaiotov et al. (1996)).

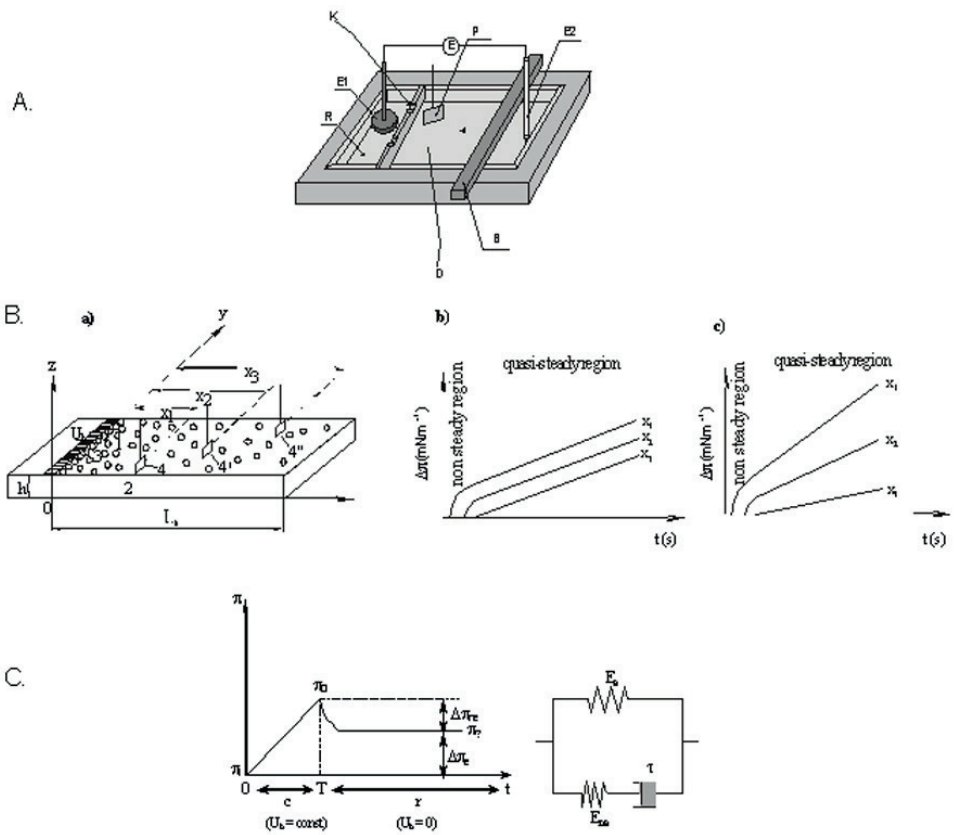

Fig. 3. A. Scheme of the used "zero order" trough: R is the reaction compartment filled with 50 cm^3, buffer pH 1.9, 11.4 or 8; D, reservoir compartment filled with double distilled water. Both compartments are communicating by means of narrow surface channel K; P – platinum Wilchelmy plate; B-teflon barrier; E1 and E2, radioactive and comparative electrode connected with the electrometer E; **B. (a)** Method of small continuous compression: (1) monolayer with length L_0; (2) aqueous sub-phase with depth h; (3) barrier moving with a constant rate U_b; 4, 4' and 4" - various distances x_1, x_2 and x_3 of the Wilhelmy plate; **(b)** $\Delta\pi(x,t)$ in an elastic monolayer; **(c)** $\Delta\pi$ (x,t) in a viscoelastic monolayer; **C.** Rheological model of the monolayer (see the text). Change of the surface pressure $\Delta\pi = \pi(t)-\pi_i$ during the time T of compression with constant velocity U_b (c) followed by a relaxation (r); π_i -initial surface pressure; π_∞ – equilibrium surface pressure.

In the absence of intrinsic surface dilatational viscosity or other relaxation processes during the compression, the rheological behavior is elastic one, obeying to Hook's law and the slops $d\pi/dt$ do not depend on the distance x (Fig.3Bb). From the $\Delta\pi(x,t)$ dependence the surface dilatational elasticity E_d can be determined.

In the case of a viscoelastic monolayer behaving like a Maxwell 2D-viscoelastic body the slops $d\pi/dt$ depend on the place of registration x (Fig. 3Bc). From the $\Delta\pi(x,t)$ dependence the characteristic time θ of the relaxation process associated with surface dilatational viscosity can be determined. The relaxation should be related to various processes, the conformational modifications of the molecules forming the surface layer being one example. The physical meaning of the relaxation rate θ^{-1} is the rate of dissipation during the compression of the accumulated elastic energy.

After stopping the compression the relaxation processes with characteristic time τ of many order of magnitudes larger than θ are observed, the reorganization of the monolayer as a whole being one example (Fig. 3C). The interpretation of the experimental data for the surface pressure change with time is based on the rheological model shown in Fig. 3C. The total surface pressure change $\Delta\pi = \pi(t)-\pi_i$ is represented as a sum of an equilibrium $\Delta\pi_e$ and a non-equilibrium $\Delta\pi_{ne}$ contribution:

$$\Delta\pi=\Delta\pi_e + \Delta\pi_{ne} \qquad (1)$$

The equilibrium part $\Delta\pi_e$ (represented by the upper branch of the mechanical model) is related to the equilibrium surface dilatational elasticity E_e. The non-equilibrium part of the total surface pressure change $\Delta\pi_{ne}$ (represented by the lower branch of the mechanical Maxwell's model) is associated with the accumulation of elastic energy during the compression and their dissipation through a slow specific molecular mechanism. From the experimental data $\Delta\pi(t)$ after stopping the rapid compression, the value for the specific time of relaxation $\Delta\pi$ and the non-equilibrium part of the total surface pressure $\Delta\pi_{ne}/\Delta\pi$ [%] were obtained.

The SUV dispersions were prepared by the Bangham method (Bangham et al., 1965), the LNC ones by the phase inversion temperature method (Heurtault et al., 2002; 2003). Post-insered LNCs were prepared using the post-insertion technique described in (Perrier et al., 2010).

The properties of molecular assemblies in the bulk of the dispersion systems before the interfacial reorganization were also studied. Determination of the size was made by photon correlation spectroscopy by using a Malvern autosizer® 4700 (Malvern Instruments Ltd., Worcesthershure, UK) fitted by a 514 nm laser beam at a fixed

angle (90°) at 25°C. The measurement of electrokinetic mobility and Zeta potential were performed by using a laser Doppler method (Malvern zetasizer® 2000, Malvern Instruments Ltd., Worcesthershure, UK) at 25 °C.

The Ptx-drug payload was measured by high performance liquid chromatography (HPLC). The transport of Ptx-loaded LNCs from the aqueous dispersion to the receptor compartment across the mucus membrane deposed on a polycarbonate membrane was studied by using a Transwell® system. The Ptx concentration in the receptor compartment and the relative coefficient of permeability $P_{\text{with mucus}}/P_{\text{without}}$ mucus were obtained [Groo et al., 2014].

Molecular model of PLA50 at A/W interface was created by using PCMODEL software (Serena Software 1993).

The morphology of the formed interfacial layers was visualized by Atomic Force Microscopy (AFM). After Langmuir Blodgett (LB) monolayer transfer from the interface on mica supports, the AFM imaging was performed with NanoScope Multi Mode V (Germany) operating in tapping mode.

Results and discussion

Small unilamellar vesicles (SUV)

When a small quantity of SUV dispersion was spread at A/W interface a process of interfacial destabilization of closed spherical vesicle (SUV) and formation of a surface film formed by partly open vesicles was observed (Launois-Surpas et al., 1992). In a simplified kinetic scheme (Fig. 4), the kinetics of the surface film formation after spreading of vesicle dispersion at the interface was described in terms of two simultaneous processes: (i) a diffusion of vesicles towards the aqueous bulk phase and (ii) a slow irreversible transformation of closed vesicles located in the zone underlying the interface into surface film formed by partly disaggregate ones.

The diffusion is described by Fick's equation, while the irreversible interfacial vesicles transformation by means of an appropriate kinetic equation similar to the Langmuir equation, neglecting desorption term:

$$\frac{dn^*}{dt} = KC(0,t)\delta\left(1-\frac{n^*}{n_\infty^*}\right) \tag{2}$$

where $n^*(t)$ is the number of partly disaggregate vesicles adsorbed on a 1 cm^2 area at time t, n_∞^* is their maximal number in closely packed layer; $(1-n^*/n_\infty^*)$ is the available surface

area at time t; δ is the vesicle diameter, *C(0,t)* is the concentration of intact vesicles in the first vesicle layer at x=0 able to be transformed, *C(0,t)*δ is the same quantity referred to a 1 cm^2 area and *K* is the transformation constant. The desorption term in the Langmuir monolayer equation is neglected because the destroyed vesicles are assumed to be completely insoluble and adsorption process to be practically irreversible.

The general case can be described by Fick's equation with boundary conditions taking the transformation process into account. The following approximation is valid for a large diffusion flow:

$$\frac{dn^*}{dt} = KC(0,t)\delta \; erf \frac{L}{2\sqrt{D\pi}}\left(1-\frac{n^*}{C_0\delta}\right) \tag{3}$$

where L is the thickness of the spread quantity (Fig. 2A) and D is the diffusion coefficient.

In presence of phospholipases, the interfacial reorganization occurs simultaneously with the phospholipolysis (Fig. 4). The appearance of the lipolytic products as a result on enzyme action destabilizes additionally the vesicles. An accelerated transformation ($\tilde{\kappa} > \kappa$) of closed spherical structures into a surface film at the air/water interface of the vesicle dispersion was then observed. The formation of the surface film is followed by measuring the interfacial properties listed above for example the evolution of the surface pressure (π) with time (*t*) at constant area (*A*) (Fig. 5).

The theoretical description of the reorganization together with the equations describing the interfacial hydrolysis of phospholipids allows us to determine the corresponding kinetic constant of reorganization *K* and overall kinetic constant of hydrolysis *Q* (Raneva et al., 1995; Mircheva et al., 2008).

Lipid nanocapsules (LNC)

It was established that there are two populations of LNC after the preparation without (LNCI), and with (LNC II) phospholipid molecules (Fig. 6) (Minkov et al., 2005a, 2005b).

Both kinds of LNC are generally stable and remain intact in the bulk of the aqueous dispersions, but at the interface of the dispersion the capsules without phospholipid molecules (LNC I population) lose their mechanical stability and undergo reorganization. A disaggregation of LNC I fraction, located in the vicinity of interface, occurs leading to the formation of a true surface film of TG from the core of LNC.

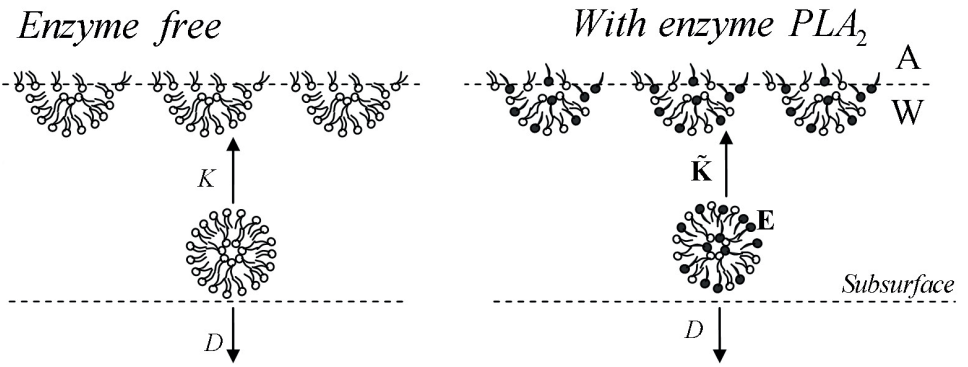

Fig. 4. Schematic representation of the diffusion and interfacial destabilization of enzyme-free SUV and SUV incubated with enzyme after spreading at A/W interface

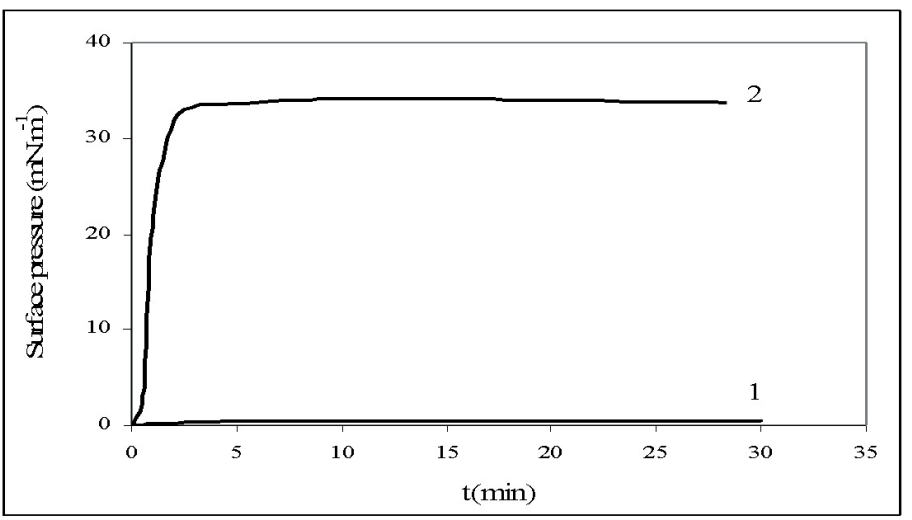

Fig. 5. Surface pressure (π) versus time (t) at A=*const* after the spreading of 100 ml DOPC vesicles: curve 1 - enzyme-free vesicle dispersion; curve 2 - vesicle dispersion pre-incubated for 1 min with enzyme; E/SUV ratio is 20:1.

As a result of the lipolytic action of phospholipase, a loss of mechanical stability of stable LNC II containing phospholipids molecules occurs and an additional spreading of released TG molecules was observed (Mircheva et al., 2008). The formation of the surface film can be followed by measuring the evolution of the surface pressure and surface potential at constant area $\pi, \Delta V(t)_A$ and the change of the surface area at constant surface pressure $\Delta A(t)_\pi$.

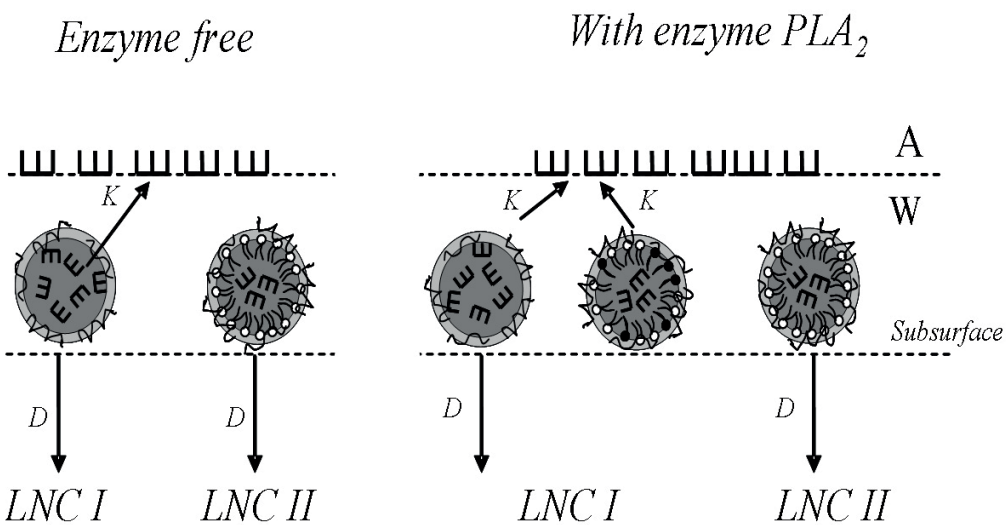

Fig. 6

Schematic representation of the diffusion and interfacial destabilization of enzyme- free LNC and LNC incubated with enzyme after spreading at A/W interface; - lipid molecule; - hydrolysis product; - TG molecule; - PEG

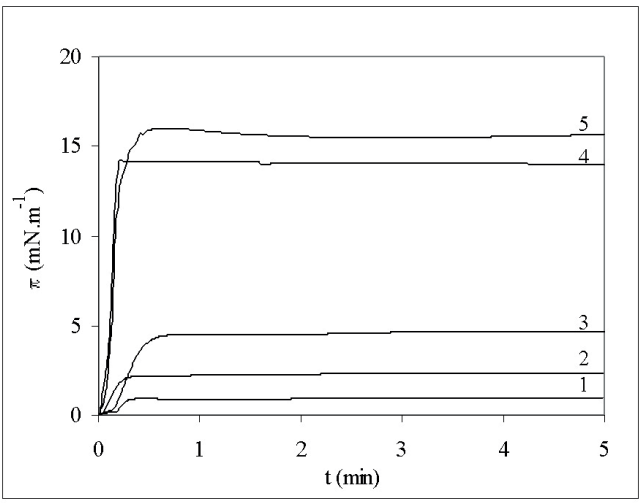

Fig. 7. Evolution of surface pressure (π) with time (t) at constant area (A) after spreading different LNCs quantities N_I (in LNC×cm^{-2}) on pure A/W interface: curve 1-N_I=0.3.10^{10}; curve 2- N_I=0.5×10^{10}; curve 3-N_I=0.8×10^{10}; curve 4- N_I=1.6×10^{10}; curve 5- N_I=3.2×10^{10}

In way of illustration Fig. 7 shows the dependence $\pi(t)_A$ resulting from LNC I interfacial disaggregation when different small LNCs quantities were spread on pure A/W interface. The values of the surface pressure (π) can be converted into values of surface concentration of spread TG molecules (Γ_{TG}) by comparison with the independently measured isotherms π(A) of pure TG monolayer. Assuming that the process of disaggregation of unstable capsules type I is rate determining, while the spreading of TG molecules confined into capsules is instantaneous, the following kinetic equation for the rate of increase of surface concentration of TG molecules can be written as:

$$\frac{d\Gamma_{TG}}{dt} = k_1 N_1 m_{TG}^0 (1-\theta) \tag{4}$$

where k_1 is the rate constant of LNCs I disaggregation; $\theta = \frac{\Gamma_{TG}(t)}{\Gamma_{TG}^{\infty}}$ is the degree of surface coverage during the monolayer formation; *(1-θ)* is the part of free surface area;

N_I is the number of unstable LNCs I per unit area; m_{TG}^0 is the number of TG molecules confined in one unstable LNC of type I; $m_{TG}^0 N_I$ is the number of TG molecules contained in all LNCs spread at unit surface.

The effectiveness (ε) of LNCs I disaggregation can be defined as the ratio between the number of spread TG molecules at A/W interface as a results of LNC I disaggregation and those contained in all spread LNCs I:

$$\varepsilon = \frac{\Gamma_{TG}^{sat}}{m_1^0 N_I} \tag{5}$$

ε_{TG} =1 obtained for the curve 1 in Fig. 7 proves that all TG contained in all spread LNCs I are spread at the interface. As in the case of SUV, the theoretical description of the coupling between the interfacial reorganization and enzyme action, allows us to determine the kinetic constant of reorganization *K* and overall kinetic constant of lipolysis *Q* (Mircheva et al., 2008). As one example the values for K and Q for SUV and LNC are compared in Table 1.

Table 1. Overall kinetic constants of disaggregation (K) and phospholipolysis (Q) of DOPC by PLA_2

Studied systems	K	*Q*
	[min^{-1}]	[$cm^3.molec^{-1}.min^{-1}$]
SUV	10	$1.9.10^{-17}$
LNC	200	$3.4.10^{-18}$

In conclusion, the comparison of the interfacial behavior of the two molecular assemblies shows that: (i) the slower interfacial reorganization of SUV leads to the formation of a surface film, formed by partly destructed vesicles, while LNC capsules release more rapidly TG molecules at the air-water interface, and a true monomolecular layer of triglyceride is formed; (ii) the comparison of the values of *Q* shows that the enzymatic catalityc act occurring at vesicle is more efficient than at nanoparticle interface. This finding is related to the differently organized assemblies of phospholipid molecules in SUV and LNC. In fact, the enzyme penetration and the mobility of phospholipid molecules are very different in differently organized interfaces and could be play also a role on the rate of the enzymatic hydrolysis.

PLA matrix

In aqueous dispersion at neutral pH the polyester particles are very stable (several months). *In vivo*, the polyesters matrix undergoes a complex slow degradation process. As far as the mechanisms of progressive degradation of particles and drugs release are concerned the discussion in the literature is largely intuitive. A contribution of prime importance of this process is the hydrolysis and scission of ester bonds and progressive appearance of water-soluble small fragments.

In order to analyze the mechanisms of polyester degradation, a simple model system-polyester monolayer spread at the A/W interface was studied. The advantage of the monolayer approach is ability to control and modify easily the interfacial organization of the ester groups and in particular the possibility to realize the optimal conditions for hydrolysis, when all ester bonds are accessible to the underlying aqueous subphase containing H^+,OH^- or enzyme (Fig. 8) (Ivanova et al., 1997a; 1997b).

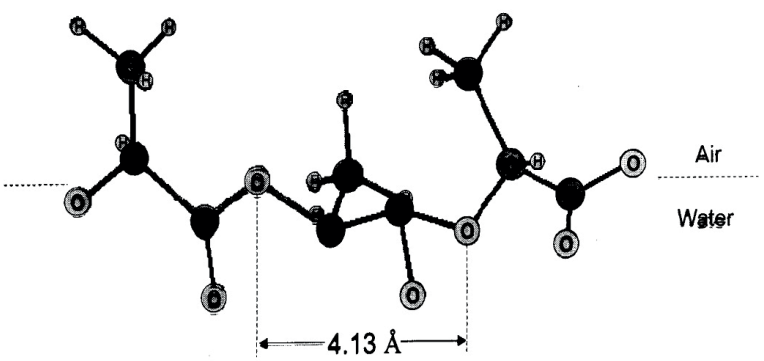

Fig. 8. Molecular model of PLA 50 at A/W interface

The course of the acidic, basic or enzymatic interfacial hydrolysis leading to the appearance of water soluble small fragments and no-soluble charged large fragment can be easily followed by using the barostat balance (Fig.9; see also Fig. 3A).

The experimental data $\Delta A(t)_{\pi}$ for acidic, basic and enzymatic hydrolysis are presented by points in Fig. 10. The theoretical prediction for $\Delta A(t)$ presented by curves is obtained by coupling the kinetic equations describing the hydrolysis together with equations describing the polymer random fragmentation process and solubilization of progressively appearant small soluble oligomers constituted by $x \leq 4$ lactic units[1)] (Ivanova

et al., 1997a; 1997b). The theoretical prediction seems to be in good agreement with experimental results at the beginning of the reaction. In the later stages of the hydrolysis, the course of the reaction at the two pH values was slowed down in comparison with the theoretical prediction. We assume that this effect is related to an inhibition process due to the accumulation at the interface of insoluble large fragment, charged negatively at pH 11.4 or positively at pH 1.9, i.e. of the same sign as the OH^- or H^+ ions respectively. The measurements of surface potential ΔV confirmed that the electrostatic repulsion was the reason for the observed deceleration of the hydrolysis process.

The values obtained for the hydrolytic rate constant k versus π of the PLA monolayers are shown in Table 2. The hydrolysis process was faster at pH 1.9 than at pH 11.4. Generally speaking, the rate of the reaction depends on the interfacial organization of lactic units. From π=2 mN.m^{-1} to π=10 mN.m^{-1}, the rate constant increased with the increase of the number of ester bonds per unit area that were able to be hydrolyzed. A maximal effect was reached at about π=10 mN.m^{-1}, corresponding to maximal close packing of all lactic groups at the interfaces (see Fig.8). The process can be visualized by AFM imaging (Fig. 11) where the morphology of condensed domains of PLA is profoundly modified after the hydrolytic process.

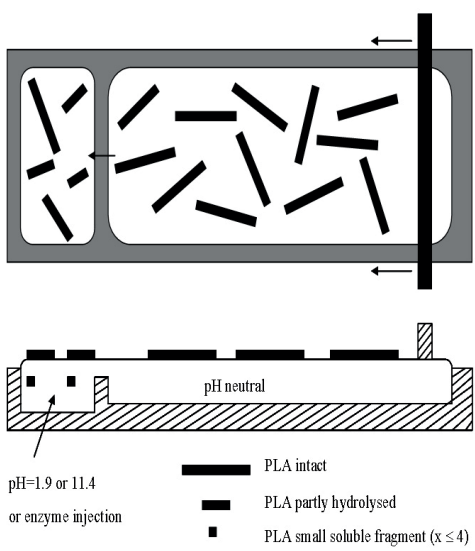

Fig. 9. Schematically representation of the fragmentation process and solubilization of small fragments in the reaction compartment containing basic or acidic solutions or enzyme The reservoir compartment is at pH neutral

In conclusion, the hydrolysis and scission of ester bonds of polyesters macromolecules leading to the appearance of water soluble oligomers are at the origin of progressive degradation in vivo of microparticles fabricated from PLA50. The study of hydrolysis of a model PLA50 monolayer at basic and acidic pH or under enzyme action demonstrates the role of the physicochemical phenomena involved in the reaction (interfacial organization of reaction species, the electric interactions between them, solubilization of the products, etc.) in the rate and mechanisms of the reaction. The developed simple approach represents an important step to better understanding the mechanism of progressive degradation of the polymer matrix and drug release *in vivo*.

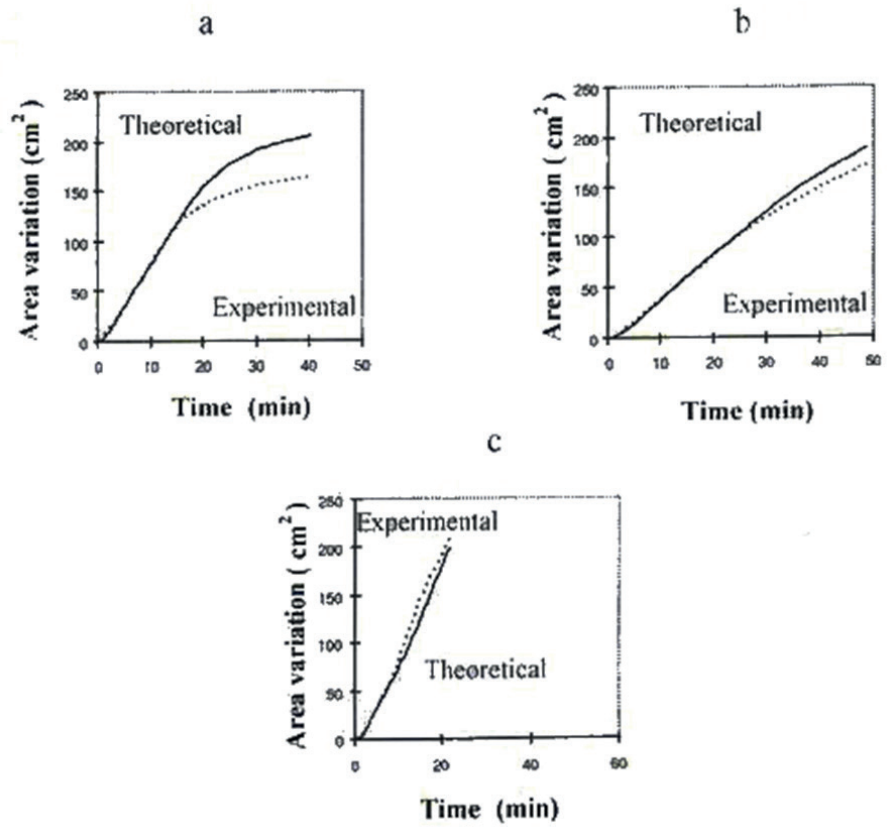

Fig. 10. Decrease of the surface area (ΔA) with time (t): (**a**) during the hydrolysis at pH 1.9; (**b**) during basic hydrolysis at pH 11.4 and (**c**) during enzymatic hydrolysis; π = 10 mN.m^{-1}: (**.**) experimental data; (-) theoretical prediction

Table 2. Hydrolytic rate constant k as a function of the surface pressure π of PLA50 monolayers

π mN.m^{-1}	k (min^{-1})	
	pH 11.4	pH 1.9
2	0.024	0.009
3	0.020	0.020
5	0.037	0.057
10	0.045	0.085
12	0.030	0.085
14.5	0.034	0.078

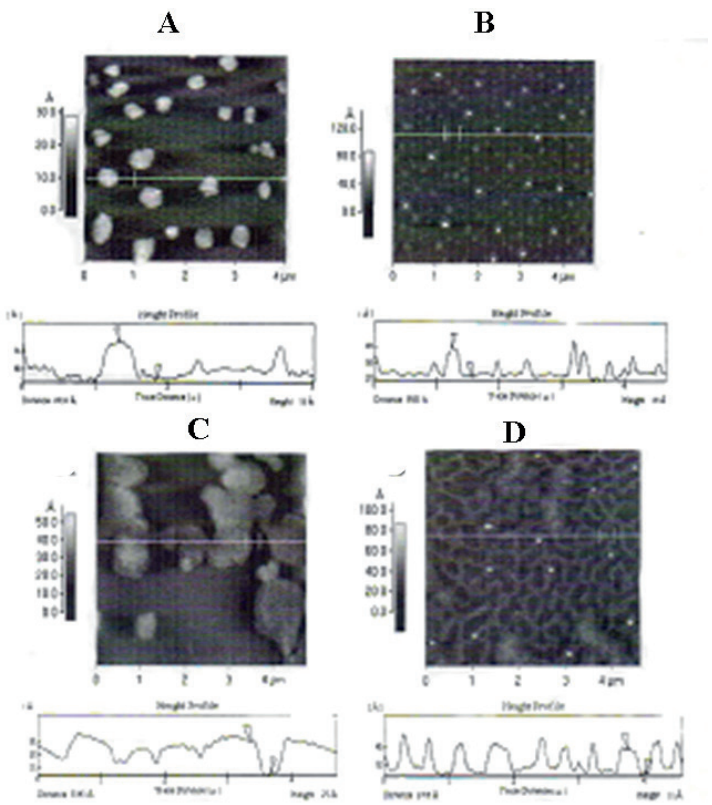

Fig. 11. AFM imaging of PLA 50 sampled at the beginning of the phase transition: (**A)** At neutral pH at Δπ= 14.5 mN.m^{-1}; (**B)** After hydrolysis at pH=11.9; (**C)** At the end of the phase transition at neutral pH and Δπ= 16 mN.m^{-1}; (**D**) After hydrolysis at pH=11.9.

Lung surfactant (LS)

It is now generally admitted (Notter, 2000; Lalchev.& Christova, 2010; Scarpelli, 1998) that a highly surface active mixture of phospholipids, neutral lipids and specific proteins is accumulated at alveolar surface of the lung. The surface active molecules are synthesized in pneumocyte II cells, stored in lamellar bodies and secreted via tubular myelin to the monolayer at the alveolar interface. The main role of the alveolar surfactant is to contribute to the maintenance of the structural stability of the alveoli during respiration by reducing the interfacial tension between the alveolar lining layer and the gas. The main component present – the saturated phospholipids DPPC is capable of achieving low surface tension and high surface elasticity but its adsorption at the interface from the organized lamellar structures, spreading and respreading into a monolayer are poor. Commercially available LSs are used clinically in the case of natural LS deficiency to restore the functions of that alveolar lining layer.

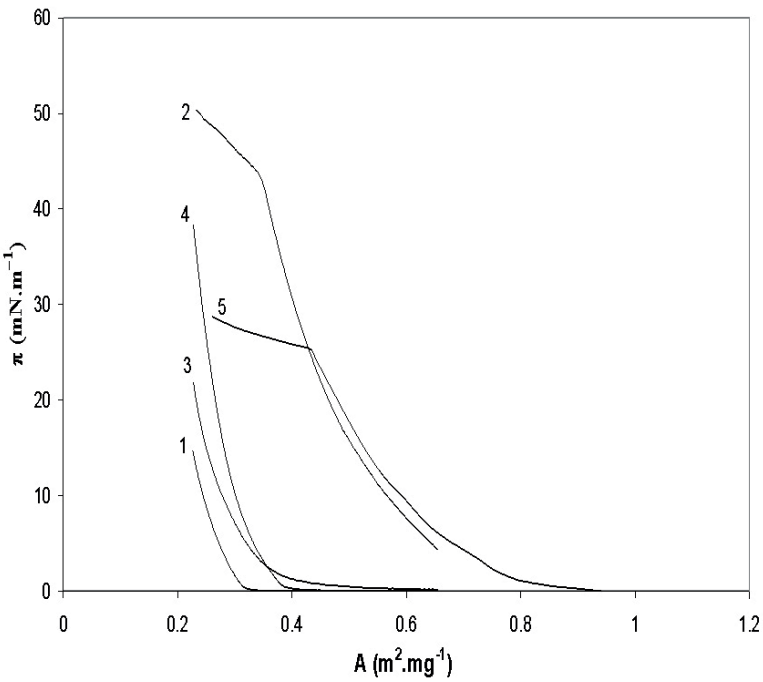

Fig. 12. π(A) isotherms of studied surfactants in comparison with the lipid fraction of total lung extract: Curve 1 - Alveofact; curve 2 - Curosurf; curve 3 - Exosurf, curve 4-Survanta; curve 5- lipid fraction of total lung extract

The study at a model A/W interface of the interfacial layers formed from spread commercially available LSs is relevant to their properties and capacity of spreading and respreading of the lamellar structures. The study of the formation and properties of the interfacial layers formed from four LSs – Alveofact, Curosurf, Survanta and Exosurf indicates that the Curosurf among the four studied LSs shows a better spreading and forms a more expanded film. The isotherms π(A) in Fig. 12 obtained from four LSs (curves 1-4) and the isotherm of lipid fraction of total lung extract (curve 5) confirms that the Curosurf (curve 2) interfacial behavior is closer to those of the lung extract.

The dilatational strains are dominant over shear strains at the alveolar surface during respiration. Therefore, a study of the dilatational properties of model monolayers of the main lipid and nonlipid compounds as well as lung surfactant monolayers seems indispensable. In order to test the effectiveness of spreading and respreading of the lung surfactants, it is convenient to measure the π(A) hysteresis at large extensions and times of deformation (Notter, 2000; Ivanova et al., 2004). By way of illustration, the first large π(A) hysteresis recorded with the four pulmonary surfactants studied spread at 40 Å^2 per molecule are presented in Fig. 13.

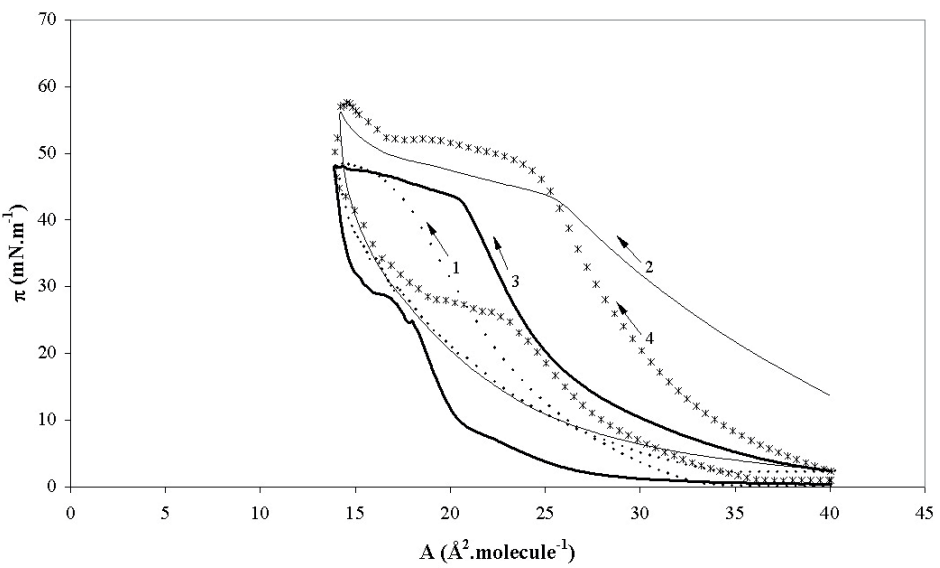

Fig. 13. π(A) large hysteresis for the studied surfactant. The initial mean area is 40 Å^2.molecule^{-1}. Curve 1 - Alveofact; curve 2- Curosurf; curve 3-Exosurf, curve 4-Survanta

The large hysteresis loops are related to the surface viscoelasticity, the solubility of soluble trace components, and mainly to the collapse and respreading of the DPPC with characteristic times commeasurable with the period T of the compression–expansion cycle. The quantitative theoretical analysis of such large π(A) hysteresis far from equilibrium is difficult, because the involved physicochemical processes are nonlinear and the surfactant chemical composition is not well known. The interfacial dilatational properties can be analyzed quantitatively by means of the rheological approach shown in Fig. 3B,C at conditions close to normal breathing (ΔA/A 10%; T 5 s). According to the rheological model from Fig. 3, an elastic behavior for all studied surfactant layers is observed during the compression. After stopping the compression, a viscoelastic behavior and relaxation processes with characteristic time τ are observed. The nonequilibrium effects due to the reorganization of the molecules with a characteristic time of about 100 s are important for Curosurf and Alveofact. The visualization of spread layers by AFM confirms that Curosurf and Alveofact show that the observed relaxation processes are due to a high effectiveness of spreading and respreading. The Fig. 14 A,B,C indicates the presence at low surface pressure of segregated zones formed by lipid molecules (A). At the collapse a coalescence of the lipid zones and protein collapsed phases (white points) are observed (B). The respreading after expansion is perfect and the aggregates disappear completely (C).

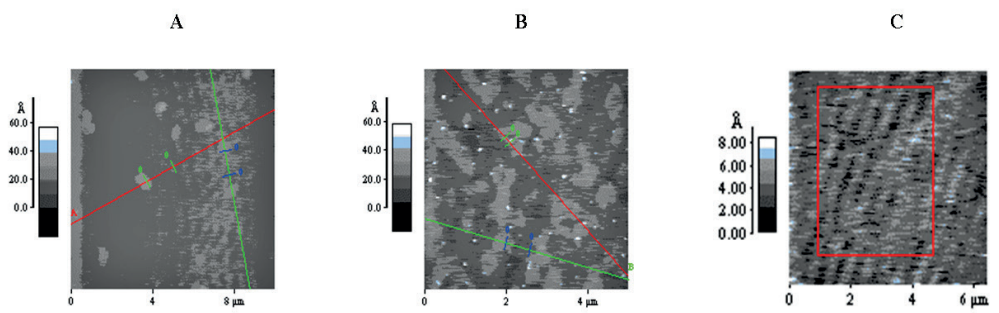

Fig. 14. AFM imaging for the Alveofact at three surface pressures: (**A**) At low surface pressures (π 5 mN.m^{-1}) before the compression-expansion cycle; (**B**) At high surface pressures (π 40 mN.m^{-1}) close to the collapse; (**C**) At low surface pressures (π 5 mN.m^{-1}) after the large compression-expansion hysteresis cycle

Table 3. Two component system BSA/LS and three component system BSA/LS/PVP at X_{PVP} =0.14

XBSA	θ-1 (s-1)		XBSA at XPVP=0.14	θ-1 (s-1)
	BSA/DPPC	BSA/Exo		BSA/Exo/PVP
0	0	0	0	0
0.25	0	0	0.22	0
0.57	0	0.13	0.49	0
0.64	1.06	0.86	0.55	0
0.77	0.95	0.98	0.66	0
0.90	-	-	0.76	0
1	0.92	0.92	0.86	7.2

It was established previously that the surface activity of the clinically used lung surfactant is reduced by serum proteins (Moses et al., 1991; Zuo et al., 2008; Zasadzinski et al., 2005) and can be restored by adding the hydrophilic polymers (Tashiro et al., 2000; Lu et al., 2002; Minkov et al., 2013). The mechanisms of lung surfactant inactivation by serum proteins and restoring effect by the hydrophilic polymers can be elucidate by means of a model study of the state and rheological dilatational properties of surface films formed from clinical lung surfactant Exosurf, Survanta, Curosurf and Alveofact in the presence of serum albumin (BSA) and hydrophilic polymers polyvinylpyrrolidone (PVP), polyethylene glycol (PEG) and Dextran. The obtained results suggest that the lung surfactant and BSA mixtures spread at air-water interface form a DPPC/BSA mixed monolayers with lower content of DPPC. The presence of hydrophilic polymers PVP, PEG and Dextran restore the DPPC content in the surface film (Minkov et al., 2013). The effectiveness of the DPPC spreading and formation of better compacted film increases in order Exosurf, Survanta, Curosurf, Alveofact. As one example the dilatational rheological behaviors of layers formed only from a poorly spreading LS - Exosurf or in mixtures with BSA in a two component or with BSA and PVP in a three component systems are summarized in Table 3 representing the dependence of the rate of relaxation during the compression (θ^{-1}) on the BSA molar fraction (X_{BSA}).

The data for a model BSA/DPPC monolayer show that the rheological response is elastic one obeying to Huck's low ($\theta^{-1} = 0$) for pure or rich in DPPC monolayer, while the pure or rich of BSA ones behaves like a Maxwell 2D-viscoelastic body with specific relaxation time ($\theta^{-1} > 0$). It should be noted that besides its poor DPPC spreading

capacity, the Exosurf layers ($X_{BSA} = 0$) similarly to the pure DPPC layers ($X_{BSA} = 0$) have one elastic behavior ($\theta^{-1} = 0$). This finding confirms the generally accepted idea that all LS form surface films containing mainly DPPC molecules.

By adding BSA to Exosurf the rheological response changes from elastic ($\theta^{-1} = 0$) to viscoelastic one ($\theta^{-1} > 0$) at composition $X_{BSA} = 0.57$, indicating the formation of a BSA/DPPC monolayer with lower content of DPPC. The addition of PVP to BSA/ Exosurf monolayer mixture restores the content of DPPC.

In conclusion, the developed approach to study the state and dilatational properties of surface layers formed at the air–water interface after spreading of dispersions containing LS pure or mixed with BSA and hydrophilic polymers would be a tool to classify the clinical lung surfactants concerning their capacity to form a compact DPPC film.

Interaction of paclitaxel-loaded LNC
with 3D and 2D model mucus membranes

This recent study is related to the oral administration of a powerful antimitotic agent Paclitaxel (Ptx) and the need to improve drug penetration through mucus of the gastrointestinal tract. Ptx was encapsulated in LNCs for oral delivery following an appropriate procedure and their stability in artificial gastrointestinal media was proved (Roger et al., 2009; Groo et al. 2013).

The mucus covers the luminal surface of the gastrointestinal tract and other tissues and constitutes an effective barrier against exogenous particles. Mucus is particularly composed of negatively charged network of mucin fibers forming a structure with pores having characteristic dimensions between 100 and 500 nm.

Three alternative mechanisms of Ptx penetration across the mucus membrane are presented in Fig. 15.

In order to answer the question which of these possibilities is predominant and to understand better the mechanisms of interactions between Ptx-loaded LNCs and mucus membrane the 3D and 2D model systems shown in the next Fig. 16 were developed (Groo et al., 2014).

In the 3D model the transport of Ptx-loaded LNCs from the donor to reservoir compartment was followed by using a Tranwell system and allows us to determine the relative coefficient of permeability $P_{\text{with mucus}}/P_{\text{without mucus}}$.

The 2D model - spreading of LNCs on a previously formed mucus monolayer at A/W interface allows us to determine the effectiveness of LNCs disaggregation ε (Groo et al., 2014; Ivanova et al., 2014).

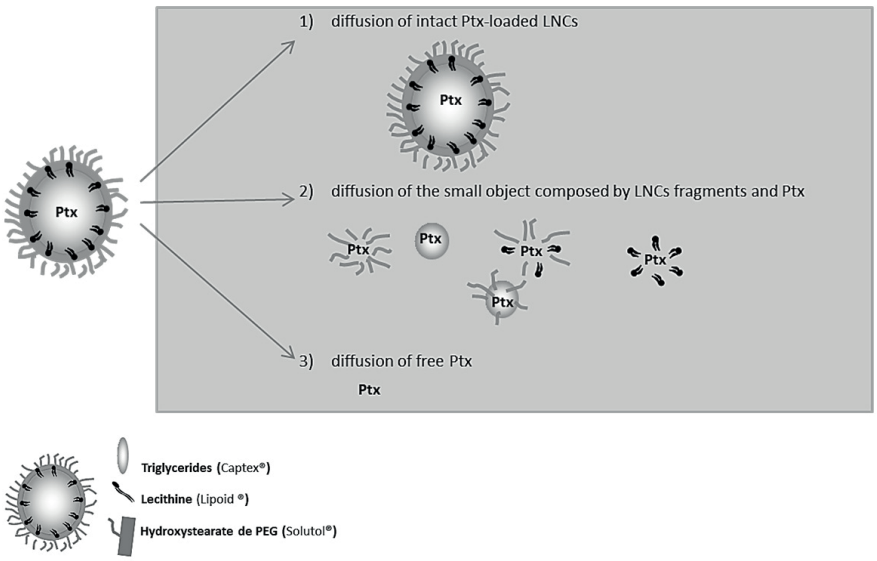

Fig. 15. Alternative mechanisms of Ptx penetration across the mucus membrane

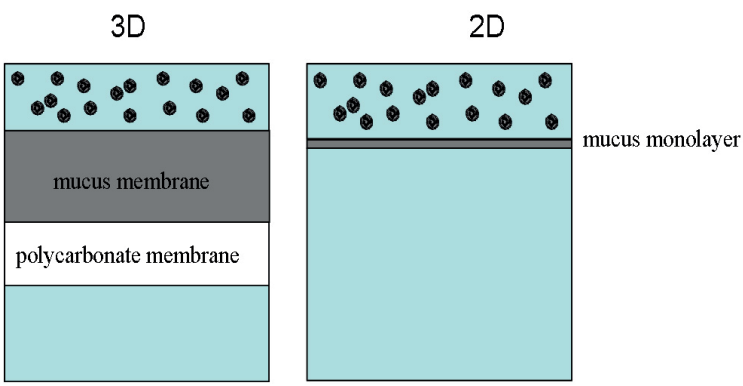

Fig. 16. 3D and 2D mucus membrane models

The results for the spreading of small LNCs quantities on previously formed mucus monolayer are compared in Fig.17 with those obtained with the monolayers formed by DPPC and Curosurf as model of the lung lining layer. By means of the developed theoretical approach from the experimental data in Fig. 17 the effectiveness (ε_{TG}) of LNCs disaggregation in interaction with the preformed model membrane monolayers

of mucus, DPPC and Curosurf were calculated and summarized in Table 4. The comparison between them shows that the LNCs spread on mucus surface layer are more stable and interact stronger with the monolayer than if they are spread on DPPC and Curosurf monolayers. These findings are in accordance with AFM images showing more 3D intact structures grafted in mucus layer than in DPPC monolayer (Fig. 18).

In order to optimize the LNCs behavior in mucus, the surface of LNCs was modified and coated with various DSPE-PEG amphiphiles by means of the so-called post-insertion process. The characteristics of all used Ptx-loaded LNCs - zeta potential (ζ), size (δ), polydispersion index (PI), drug payload were controlled. The results arranged from more positively to more negatively charged LNC are presented in the next Table 5. At the same Table the values for relative coefficient of permeability $P_{\text{with mucus}}/P_{\text{without mucus}}$, obtained from 3D model system and for the effectiveness of LNCs disaggregation ε obtained from 2D model system are presented.

The size (δ) of all used LNCs have been approximately the same and smaller than the pores of mucus membrane, they can not be responsible for the observed differences in the $P_{\text{with mucus}}/P_{\text{without}}$. The membrane permeability is larger for positive or neutral LNC. That makes us think that the better permeability is partially due to the electrostatic interactions between positively charged LNC and negatively charged mucus network. Another effect on the permeability across the mucus membrane related with the increase of LNCs hydrophilicity in the order of PEG 2000, PEG 3000 and PEG 5000 is observed.

It is interesting also to note that the permeability coefficient for all studied LNC is better in comparison with those obtained with used in clinical practice - Taxol®.

The developed 2D A/W interfacial model even that is not corresponding to the intestinal luminal interface brings some useful complementary information about the interaction between LNCs with variously modified interfaces and mucus layer. As we can see, the positively charged LNCs surfaces are attracted by negatively charged mucus monolayer and in close contact with A/W interface show high values of the effectiveness of disaggregation. As one example for LNC-DSPE-PEG 2000-amino, ε 0.90 is close to the situation corresponding to ε= 1 when all spread LNCs were disaggregated.

In conclusion, the anticancer drug Paclitaxel (Ptx) was encapsulated in LNCs with variously modified surfaces to improve the drug penetration across the mucus gastrointestinal membrane. The properties of such particles as zeta potential, size, drug payload etc are compared with the results obtained on basis of 3D and 2D mucus membrane model systems. From the 3D model system the relative coefficients of membrane permeability for all studied LNCs were obtained, while the 2D model system brings some additional information about the interaction between the LNCs and mucus

layer. The developed approach constitutes an efficient screening method to select the most favorable Ptx-loaded LNCs for mucus penetration. The model study shows that the penetration potential of positive or neutral formulations with shorter PEG chains is better then for the other studied modified LNCs.

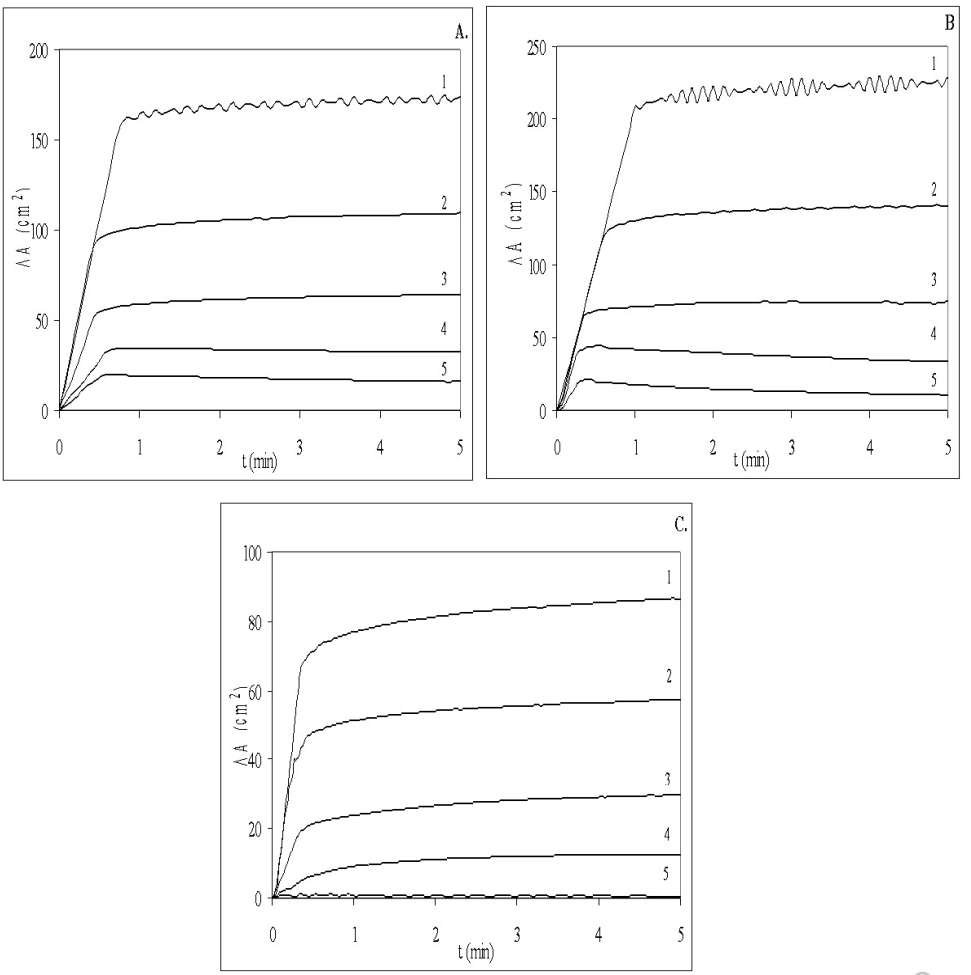

Fig. 17. ΔA(t) after spreading of LNCs on previously formed: (**A**) DPPC, (**B**) Curosurf and (**C**) mucus monolayers at various constant surface pressure: curve 1- π=5 mN.m^{-1}; curve 2 - π=10 mN.m^{-1}; curve 3 - π=15 mN.m^{-1}; curve 4 - π=20 mN.m^{-1}; and curve 5-π=25 mN.m^{-1}

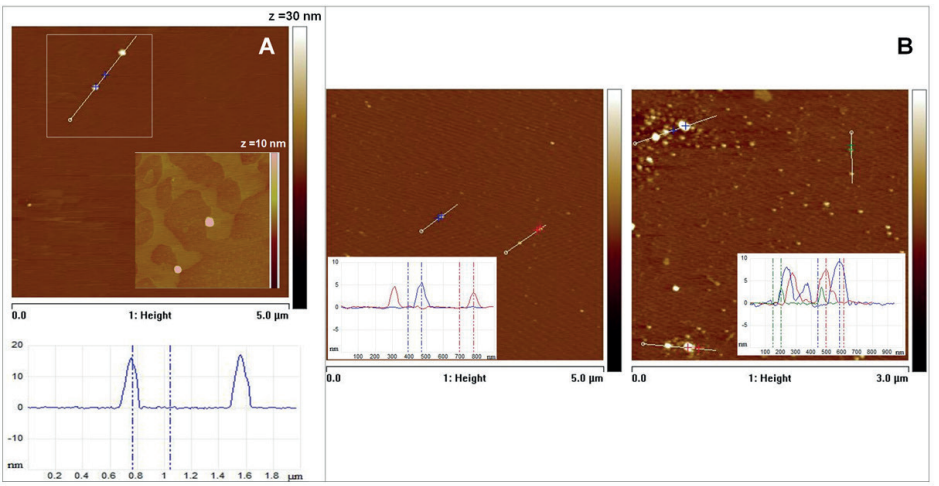

Fig. 18. (A) AFM topography images of LB films transferred from DPPC monolayer compressed to π=5 mN.m^{-1} followed by deposition of LNC dispersion (the inset is area zoom with z=10nm). Beneath, cross-section of LNCs, embedded into DPPC; **(B)** AFM topography images of LB films of pure mucus monolayer (left image) and AFM image of LB film from preformed mucus monolayer with LNCs (right image). The insets are particular cross/sections

Table 5. Characteristics of all used Ptx-loaded LNCs - zeta potential (ζ), size (δ), polydispersion index (PI), coefficient of permeability $P_{with\ mucus}/P_{without\ mucus}$, surface pressure (π) and effectiveness of LNCs I disagregation (ε_{TG})

Type LNC	Characterization LNC				3D-model	2D-model	
	ζ -potential (mV)	δ (nm)	PI	Concentration Ptx (mg.g^{-1})	$\frac{P_{with\ mucus}}{P_{without\ mucus}}$	π (mN.m^{-1})	ε_{TG}
LNC-chitosan	25.3	67.1	0.182	1.90	0.53	5 10 15	
LNC-DSPE-PEG2000-amino	4.3	67.1	0.064	1.89	0.45	5 10 15	0.92 0.86 0.90

LNC	-7.6	56.2	0.038	1.98	0.45	5 10 15	0.49 0.29 0.14
LNC-DSPE-PEG5000-amino	-16.5	75.1	0.102	1.83	0.29	5 10 15	0.07 0.03 0.01
LNC-DSPE-PEG3000-methoxy	-20.4	65.3	0.070	1.87	0.37	5 10 15	
LNC-DSPE-PEG2000-methoxy	-27.2	62.6	0.077	1.88	0.41	5 10 15	0.21 0.10 0.03
LNC-DSPE-PEG2000-methoxy	-35.7	64.1	0.006	1.89	0.31	5 10 15	0.17 0.12 0.05
Taxol					0.23		

Finally, the developed in a series of investigations simple model systems represent an important first step to assess the behavior of various kinds of micro- and nanosized molecular assemblies as drug carriers on interfacial networks in the living environment. They has provided new information about the mechanisms of interfacial reorganization and drug delivery of SUV, LNC, polyester matrix and LS carriers in the complex living systems. Together with the analyse of the behavior of drug carriers in model systems closer to the *in vivo* situation as well as with *in vivo* experiments, the developed simple models contribute to better understanding of the behavior *in vivo* and to select the most efficient formulation of DDS.

Abbreviations:

DDS- drug delivery system; MA-molecular assemblies; SUV- small unilamellar vesicles; LNC- lipid nanocapsules; TG- triglycerides; PEG- polyethylene glycol; PLA 50- Poly (D,L-lactic acid);LS-lung surfactant; Ptx-Paclitaxel; A/W-air/water; O/W-oil//water; IL-interfacial layer; PVP- polyvinylpyrrolidone; BSA-serum albumin; PLA_2-phospholipase A_2

NOTES

1. Vert M., personal communication.

REFERENCES

Arun Rasheed, Ashok Kumar, C.K. & Sravanthi, V.V.N.S.S. (2008). Cyclodextrins as drug carrier molecule: a review. Sci. Pharm., 76, 567–598.

Bangham, A.D., Standish, M.M. & Watkins, J.C. (1965). Diffusion of univalent ions across the lamellae of swollen phospholipids. J. Mol. Biol. 13, 238-252.

Blanco, O. & Pérez-Gil, J. (2007). Biochemical and pharmacological differences between preparations of exogenous natural surfactant used to treat respiratory distress syndrome: role of the different components in an efficient pulmonary surfactant. Eur. J. Pharmacol., 568, 1–15.

Dimitrov, D.S., Panaiotov, I., Richmond, P. & Ter-Minassian Saraga, L. (1978). Dynamics of insoluble monolayers – I: dilatational or elastic modulus, friction coefficient and Marangoni effect for dipalmitoyllecithin monolayers., J. Colloid & Interface Sci. 65, 483-494.

Ducel, V., Richard, J., Saulnier, P., Popineau, Y. & Boury, F., (2004). Evidence and characterization of complex coacervates containing plant proteins: application to the microencapsulation of oil droplets. Colloids Surf. A, 232, 239–247.

Glowka, E., Sapin-Minet, A, Leroy, P, Lulek, J & Maincent, P. (2010). Preparation and in vitro-in vivo evaluation of salmon calcitonin-loaded polymeric nanoparticles. J. Microcapsul., 27, 25-36.

Groo, A.C, Saulnier, P, Gimel, J.C, Gravier, J, Ailhas, C, Benoit, P. & Lagarce, F. (2013). Fate of paclitaxel lipid nanocapsules in intestinal mucus in view of their oral delivery. Int. J. Nanomedecine, 8, 4291–4302.

Groo, A.C., Mircheva, K., Bejaud, J., Ailhas, C., Panaiotov, I., Saulnier, P., Ivanova Tz. & Lagarce, F. (2014). Development of 2D and 3D mucus models and their interactions with mucus penetrating paclitaxel-loaded Lipid nanocapsules, Pharmac. Res., 31, 1753-1765.

Heurtault, B, Saulnier, P., Pech, B, Proust, J.E. & Benoit, J.P. (2002). A novel phase inversion-based process for the preparation of lipid nanocarriers. Pharm. Res., 19, 875-880.

Heurtault, B, Saulnier, P, Pech, B, Venier-Julienne, M.C, Proust, J-E, Phan-Tan-Luu, R. & Benoit, J.P. (2003). The influence of lipid nanocapsule composition on their size distribution. Eur. J. Pharm. Sci., 18, 55-61.

Ivanova, Tz., Panaiotov, I., Boury, F., Proust, J.E., Benoit, J.P. & Verger, R.(1997a). Hydrolysis kinetics of poly(D,L-lactide) monolayers spread on basic or acidic aqueous subphases, Colloids Surf. B, 8, 217-225.

Ivanova, Tz., Panaiotov, I., Boury, F., Proust, J.E. & Verger, R. (1997b). Enzymatic

hydrolysis of poly(D,L-lactide) spread monolayers by cutinase. Colloid & Polymer Sci., 275, 449-457.

Ivanova, Tz., Minkov, I., Panaiotov, I., Saulnier, P. & Proust, J.E. (2004). Dilatational properties and morphology of surface films spread from clinically used lung surfactants. Colloid & Polymer Sci., 282, 1258–1267.

Ivanova, Tz., Mircheva, K., Balashev, K., Minkov, I., Saulnier, P. & Panaiotov, I. (2014). Interfacial behavior of lipid nanocapsules spread on model membrane monolayers. Colloid & Polymer Sci, 292, 1307-1318.

Kumari, A., Yadav, S.K.& Yadav, S.C. (2010). Biodegradable polymeric nanoparticles based drug delivery systems. Colloids Surf. B, 75, 1-18.

Lalchev, Z. & Christova, E. (2010). Alveolar surfactant and neonatal respiratory distress syndrome. Sofia: University of Sofia Press [In Bulgarian].

Launois-Surpas, M.A., Ivanova, Tz., Panaiotov, I., Proust, J.E., Puisieux, F. & Georgiev, G. (1992). Behavior of pure and mixed DPPC liposomes spread or adsorbed at the air-water interface. Colloid & Polymer Sci. 27, 901-911.

Lu, J.J, Cheung, W.W.Y., Yu, L.M.Y., Policova, Z, Li, D, Hair, M.L. & Neumann, A.W. (2002). The effect of dextran to restore the activity of pulmonary surfactant inhibited by albumin. Respir. Physiol. Neurobiol. 130, 169–179.

Makadia, H.K. & Siegel, S.J. (2011). Poly lactic-co-glycolic acid (PLGA) as biodegradable controlled drug delivery carrier. Polymer, 3, 1377-1397.

Malzert-Fréon, A., Saint-Lorant, G., Hennequin, D., Gauduchon, P., Poulain, L. & Rault, S. (2010). Influence of the introduction of a solubility enhancer on the formulation of lipidic nanoparticles with improved drug loading rates. Eur. J. Pharm. & Biopharm., 75, 117 - 127.

Minkov, I., Ivanova, Tz., Panaiotov, I., Proust, J.E. & Saulnier, P. (2005b). Reorganisation of lipid nanocapsules at air-water interface: 2 - properties of the formed surface film. Colloids Surf. B, 44, 197-123.

Minkov, I., Ivanova, Tz., Panaiotov, I., Proust, J.E. & Saulnier, P. (2005a). Reorganisation of lipid nanocapsules at air-water interface: 1 - kinetics of surface film formation. Colloids Surf. B, 45, 14-23.

Minkov, I., Mircheva, K., Grozev, N., Ivanova, Tz. & Panaiotov, I. (2013). Properties of mixed monolayers of clinical lung surfactant, serum albumin and hydrophilic polymers. Colloids Surf. B, 101, 135– 142.

Mircheva, K., Minkov, I., Ivanova, Tz., Panaiotov, I., Proust, J.E. & Verger, R.(2008). Comparative study of lipolysis by PLA_2 of DOPC substrates organized as monolayers, bilayer vesicles and nanocapsules, Colloids Surf. B, 67, 107-114.

Moses, D, Holm, B.A, Spitale, P, Liu, M.Y & Enhorning, G. (1991). Inhibition of pulmonary surfactant function by meconium. Am. J. Obstet. Gynecol., 164, 477–481.

Notter, R.H. (2000). Lung surfactants: basic science and clinical applications. New York: Marcel Dekker.

Panaiotov, I., Dimitrov, D.S. & Ter-Minassian Saraga, L.(1979). Dynamics of insoluble monolayers – II: viscoelastic behaviour and Marangoni effect for mixed protein phospholipid films. J. Colloid & Interface Sci. 72, 49-53.

Panaiotov, I., Ivanova, Tz., Proust, J.E., Boury, F., Denizot, B., Keough, K. & Taneva, S. (1996). Effect of hydrophobic protein SP-C on structure and dilatational properties of the model monolayers of pulmonary surfactant.Colloids Surf. B, 6, 243-260.

Perrier, T, Saulnier, P, Fouchet, F, Lautram, N & Benoit, J.P. (2010). Post-insertion into lipid nanocapsules (LNCs): from experimental aspects to mechanisms. Int. J. Pharm., 396, 204–209.

Raneva, V., Ivanova, Tz, Verger, V. & Panaiotov, I. (1995). Comparative kinetics of phospholipase A_2 action on liposomes and monolayers of phosphatidylcholine spread at the air-water interface. Colloids Surf. B, 3, 357-369.

Roger, E, Lagarce, F & Benoit, J.P. (2009).The gastrointestinal stability of lipid nanocapsules. Int. J. Pharm., 379, 260-265.

Scarpelli, E.M. (1998). Surfactants and the lining of the lung. Baltimore: Johns Hopkins University Press.

Sharma, A. & Sharma, U.S. (1997). Liposomes in drug delivery: progress and limitations. Int. J. Pharm., 154, 123-140.

Szoka, F.C. (1991). Liposomal drug delivery: current status and future prospects (pp.845-890). In: Wilschut, J. & Hoekstra, D. (Eds.). Membrane fusion. New York: Marcel Dekker.

Tashiro, K, Kobayashi, T & Robertson, B. (2000). Dextran reduces surfactant inhibition by meconium. Acta Paediatr., 89, 1439–1445.

Verger, R. & de Haas, G. (1973). Enzyme reactions in a membrane model 1: a new technique to study enzyme reactions in monolayers. Chem. Phys. Lipids. 10, 127-136.

Yuan, C., Jin, Z., Xu, X., Zhuang, H. & Shen, W. (2008). Preparation and stability of the inclusion complex of astaxanthin with hydroxypropyl-b-cyclodextrin. Food Chem., 109, 264–268.

Zaibunnisa, A.H., Aini Marhanna, M.N.A. & Ainun Atirah, M. (2011). Characterisation and solubility study of γ-cyclodextrin and β-carotene complex. Int. Food Res. J., 18, 1061-1065.

Zasadzinski, J.A., Alig, T.F., Alonso, C., Bernardino de la Serna, J., Perez-Gil, J. & Taeusch, H.W. (2005). Inhibition of pulmonary surfactant adsorption by serum and the mechanisms of reversal by hydrophilic polymers: theory. Biophys. J., 89, 1621–1629.

Zuo, Y.Y., Vedhuizen, R.A., Neumann, A.W., Petersen, N.O. & Possmayer, F. (2008). Current perspectives in pulmonary surfactant--inhibition, enhancement and evaluation. Biochim. Biophys. Acta, 1778, 1947-1977.

✉ **Prof. Dr. Tz. Ivanova** (corresponding author)
Biophysical Chemistry Laboratory,
Department of Physical Chemistry
University of Sofia
1, James Bourchier Blvd.
1164 Sofia, Bulgaria
E-mail: tzivanova@chem.uni-sofia.bg